

Structural and Functional Changes of the Right Ventricle in Sprague Dawley and Wistar Rat Models of Pulmonary Arterial Hypertension

Liomar A. A. Neves¹, Paola C. Rosas², Hongjian Wang¹, Peter B. Senese¹, Michael R. Gralinski¹

¹CorDynamics, Inc., Chicago, IL; ²College of Pharmacy, University of Illinois at Chicago, Chicago, IL

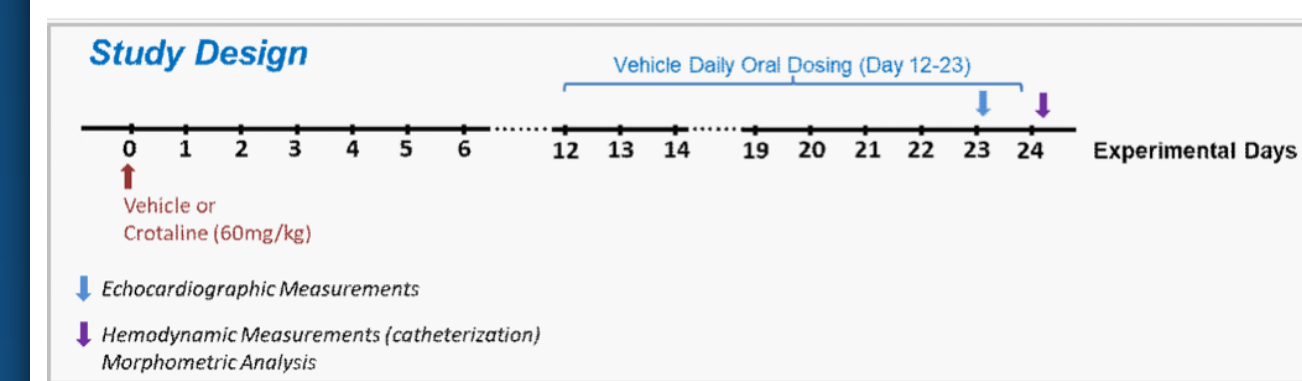
Introduction

PAH (pulmonary arterial hypertension) is a progressive disease characterized by increased pulmonary vascular resistance and consequently, right ventricular remodeling, hypertrophy and failure. Despite the advances in treatment for PAH during the past few decades, there is still a poor 5-year survival rate for newly diagnosed patients. In recent years, emerging therapeutic modalities have focused on disease-modifying agents that can impact the multifactorial pathophysiology of the vascular remodeling occurring in PAH in the hope of disrupting the disease and improving long term survival.

The efficacy of new treatments often centers around the terminal assessment of a test compound on right ventricle (RV) pressure without considering the evaluation of RV morphology and function. The use of noninvasive and non-terminal imaging techniques is crucial for a comprehensive examination of disease progression in animal models. Transthoracic echocardiography remains the standard approach to evaluating heart morphology and function in animal models due to its low cost and ease of use compared to other imaging modalities such as magnetic resonance imaging.

Animal models of PAH are invaluable tools in assessing the efficacy of new drug treatments. The monocrotaline (MCT)-induced PAH rat model is characterized by remodeling of the pulmonary arterial vessels, which in turn leads to increased pulmonary vascular resistance and right ventricular hypertrophy. Depending on the MCT dose, age and strain of the animals, the RV hypertrophy will progress into failure within weeks. Sprague Dawley rat (SDR) and Wistar rat strains are commonly used in MCT-induced pulmonary hypertension models; however, little is known about the differences between these strains in response to MCT. Therefore, in this study we use echocardiography and RV catheterization to compare the RV functional, structural and hemodynamic changes in response to MCT in SDR and Wistar rats.

Methods



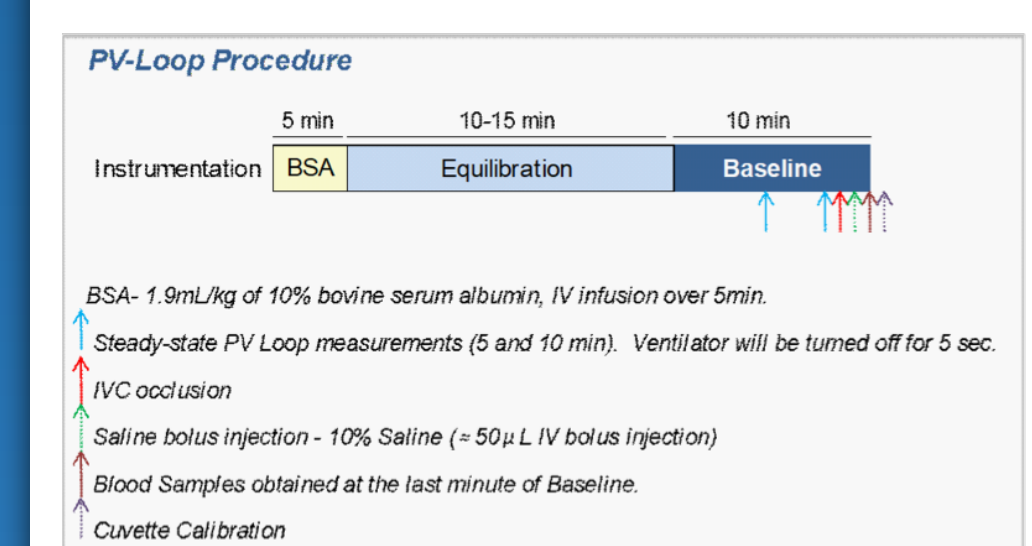
SDR and Wistar rats (194-243 g) were divided into 4 groups: Vehicle/SDR, MCT/SDR, Vehicle/Wistar and MCT/Wistar. On Study Day 0, rats in the MCT groups received a subcutaneous dose (3 mL/kg) of monocrotaline (60 mg/kg in HCl/NaOH, pH 7.4) while rats in the vehicle groups received a subcutaneous dose of 0.9% sodium chloride for injection, U.S.P or deionized water pH 7.4. All rats received vehicle (0.2% HPMC [hydroxypropyl methyl cellulose] in deionized water or just deionized water) daily via oral gavage from Study Days 12 to 23. Cage-side observations for general health and appearance were performed once daily.

Echocardiographic measurements: On Study Day 23, RV structure and function were assessed by echocardiography in rats under isoflurane (1–2%) anesthesia. Transthoracic echocardiography was performed using a Vevo 2100 (Visual Sonics, Toronto, ON, Canada) equipped with a 21-MHz solid state transducer (MS250S). Body temperature and heart rate were monitored throughout the procedure.

Hearts were initially imaged in the modified parasternal long-axis view of the RV outflow tract and the M-mode window was positioned to go through the widest portion of the RV chamber using the aorta as a landmark. The following parameters were obtained from the M-mode once in this position: right ventricle internal diameter during diastole (RVIDd), right ventricle internal diameter during systole (RVIDs) and right ventricle free wall thickness (RVFWT, measured during end-diastole). Then probe angle was adjusted until the pulmonary valve (PV) was clearly visualized, and the PV diameter was obtained. The pulmonary velocity time integral (PV TI) was also obtained, and the cardiac output (PVC0) and stroke volume (PVSV) were calculated. The PAT/PET and PAT/CL ratio were obtained.

The apical four-chamber view of the right side of the heart was obtained to simultaneously view the RV and right atrium (RA). The RA area was obtained from the b-mode image at end-systole and end-diastole. The RV end-diastolic area (RVEDA) and RV end-systolic area (RVESA) were obtained from the apical four-chamber view of the right ventricle, and the fractional area change calculated [(RVEDA-RVESA)/RVEDA]. Tricuspid valve flow patterns were assessed in the apical four-chamber view by PW Doppler, and the peak velocities of flow in the early phase of diastole (E), tricuspid closure open time (TCO) and ejection time (ET) obtained. The RV index of myocardial performance (RVMPI) was calculated using the formula: (TCO-ET)/ET. Additionally, the tricuspid annular velocity at early diastole (E') and the tricuspid annular velocity at systole (S') were obtained with the sample volume at the free wall side of the tricuspid annulus in the four-chamber view. The E'/E' ratio was calculated. The M-mode doppler beam was placed through the lateral annulus of the tricuspid valve plane to obtain the tricuspid annular plane systolic excursion (TAPSE).

Echocardiographic images were analyzed off-line using VevoLab Software (version 5.7.1). Measurements and calculations were averaged from 3 consecutive cycles and performed according to the American Society of Echocardiography guidelines.



Hemodynamic Measurements: On Study Day 24, all rats were anesthetized with isoflurane, ventilated and the systemic arterial pressure, HR and LV pressure-volume loop (PV loop) were assessed by catheterization.

An incision was made below the xyphoid process, and the apex of the heart exposed. The apical RV free wall was punctured, and a Millar pressure-volume catheter (SPR-869, 2F) tip was introduced retrograde through the stab incision until the proximal electrode on the catheter was just inside the ventricle wall. The catheter was adjusted to obtain consistent shaped loops. The Millar pressure-volume catheter was used to measure RV pressure, volume and HR.

The inferior vena cava (IVC) was isolated below the diaphragm and a piece of silk suture placed underneath the IVC and a loose knot tied. The right femoral vein was also isolated, ligated anteriorly and cannulated for BSA administration and saline calibration.

After instrumentation, approximately 1.9 mL/kg of 10% BSA in saline was infused over 5 minutes into a femoral vein to compensate for blood loss during surgery. The equilibration period (approximately 10–15 minutes) started after the BSA administration. Once all parameters reached steady state, baseline measurements were collected for 10 minutes. At 5 and 10 minutes into the baseline, a 5-second period of apnea was induced for steady-state analysis of the pressure-volume parameters.

At the end of baseline period, IVC occlusion was performed. The suture placed under the IVC was held by both ends with a needle clamp and gently raised over 1–2 seconds and then the tension was slowly released. IVC occlusion was performed during a period of apnea and repeated until at least 2 separate optimal recordings were made. The ventilator was stopped during IVC occlusion.

After IVC occlusion, a parallel conductance (Vp) value was obtained by injecting 50–80 µL bolus of hypertonic saline (10% sodium chloride) into the femoral vein. The saline bolus was repeated until 1–2 separate optimal recordings were made. The ventilator was stopped during saline bolus injection.

Right ventricular pressure and volume was monitored with the LabChart Pro (ADInstruments, Colorado Springs, CO) v8.1 data capture system. Volume parameters were converted into µL units using the cuvette and saline bolus calibration. The RV pressure and volume parameters were obtained as a 13-cycle average during each apnea period (5–10 minutes of baseline). The CO values obtained from the RV pressure and volume and echocardiographic assessments were used to determine the alpha calibration factor. The RV pressure and volume parameters were reanalyzed after applying the alpha factor. Parameters obtained during IVC occlusions are averages of at least 2 measurements.

Morphometric Analysis: The rats were euthanized by exsanguination after the hemodynamic measurements; the heart-lung block was removed and gently infused with the vasculature with ice cold saline until the perfusate ran clear. The heart and lungs were separated, aorta removed, excess saline drained, and each organ weighed separately. The atria were removed and discarded. The left ventricle with septum (LV+S) was separated from the RV. The ventricles were weighed separately. The left tibia was removed and separated from the soft tissue. A longitudinal measurement was obtained with a digital caliper.

Objectives

To compare RV function, structure and hemodynamics in response to MCT in SDR and Wistar rats.

Results

Figure 1. MCT Treatment Resulted in RV Hypertrophy in SDR and Wistar Rats, but Greater Hypertrophy Was Shown in SDR

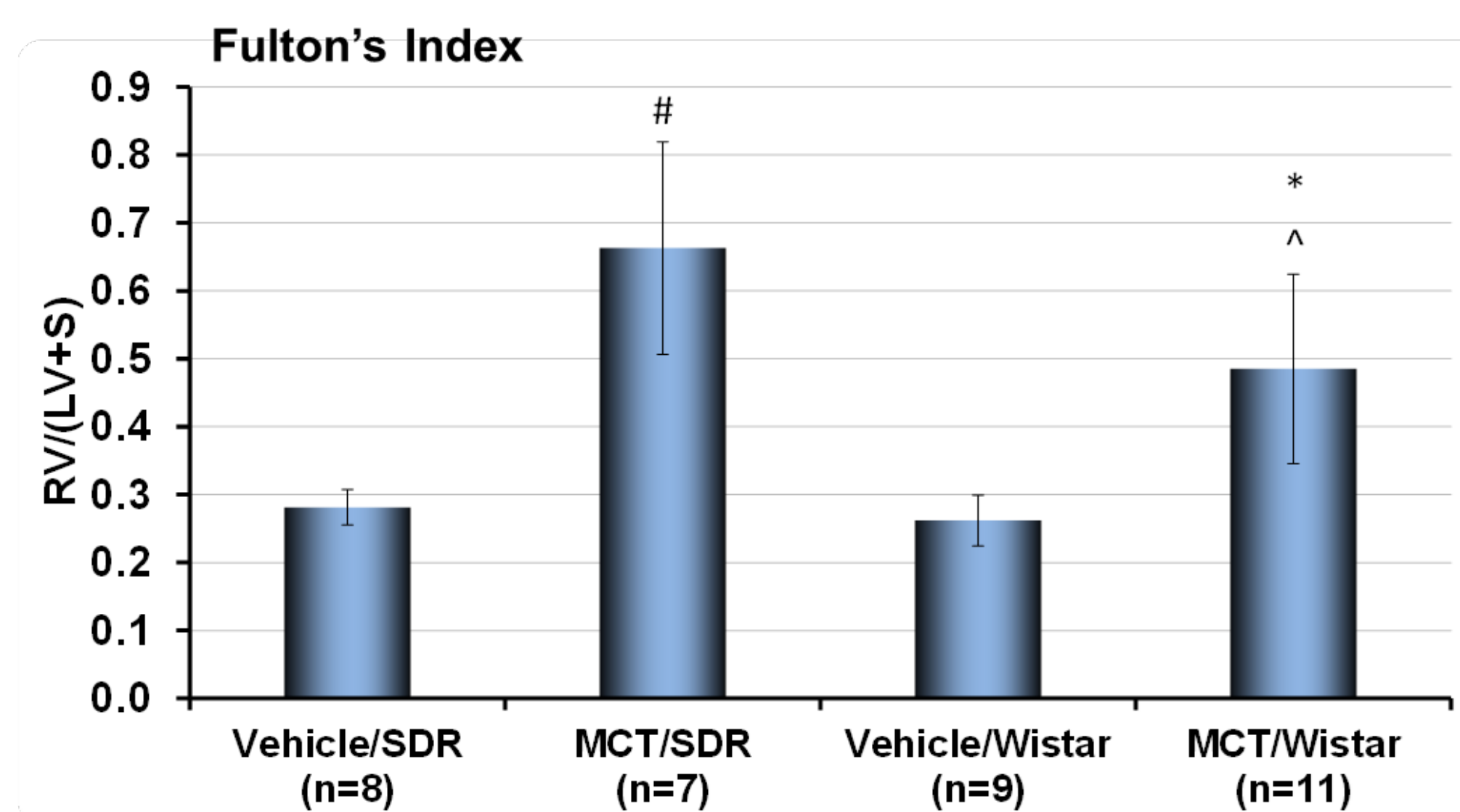


Table 1. MCT-induced Increase in RV Hypertrophy Was Greater in SDR

| Morphometric Parameters | Experimental Groups | | | |
|-------------------------|---------------------|---------------------------|---------------------------|----------------------------|
| | Vehicle/SDR | MCT/SDR | Vehicle/Wistar | MCT/Wistar |
| | n=8 | n=7 | n=9 | n=11 |
| mean ± SD | mean ± SD | mean ± SD | mean ± SD | mean ± SD |
| HW/TL (mg/mm) | 29.41 ± 2.40 | 30.81 ± 3.22 | 22.00 ± 1.91 [†] | 23.22 ± 3.83 [^] |
| LW/TL (mg/mm) | 40.29 ± 2.03 | 55.77 ± 6.75 [†] | 36.99 ± 2.35 | 54.86 ± 14.24 [*] |
| (LV+S)/TL (mg/mm) | 20.55 ± 1.81 | 16.11 ± 1.00 [†] | 15.44 ± 1.34 [†] | 13.99 ± 1.77 [^] |
| RV/TL (mg/mm) | 5.76 ± 0.53 | 10.65 ± 2.39 [†] | 4.04 ± 0.68 | 6.80 ± 2.14 ^{*^} |
| TL (mm) | 39.32 ± 1.03 | 38.73 ± 1.74 | 37.69 ± 1.87 | 37.18 ± 2.50 |

[†] p < .05 vs Vehicle/SD; ^{*} p < .05 vs Vehicle/Wistar; [^] p < .05 vs MCT/SD. SDR, Sprague Dawley; HW, heart weight; LW, lung weight; LV + S, left ventricle + septum; RV, right ventricle; TL, tibia length; MCT, monocrotaline (60 mg/kg) as a single dose administered on Day 0.

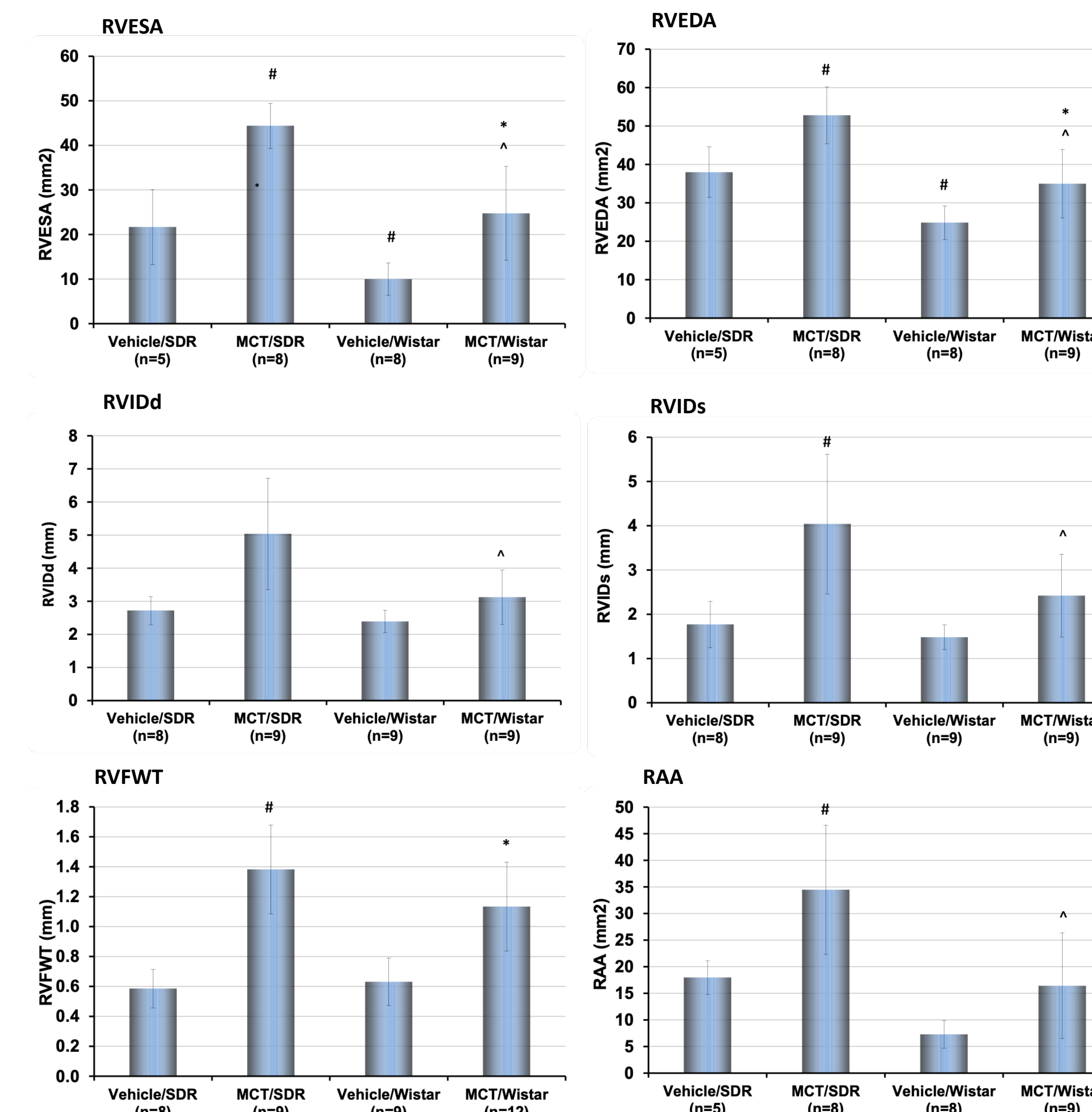
MCT treatment resulted in RV hypertrophy in SDR and Wistar rats as shown by an increase in Fulton index (RV weight normalized to LV + Septum weight) and RV weight normalized to tibia length. Greater hypertrophy was observed in SDR as compared to Wistar rats.

Left ventricle + septum weight normalized to tibia length ratio was decreased in MCT/SDR as compared vehicle control, but unchanged in MCT/Wistar rats.

Pulmonary congestion was observed with MCT treatment as shown by an increase in the lung weight to tibia length ratio in both strains as compared with the respective vehicle controls.

Values are expressed as mean ± SD. # p < .05 vs Vehicle/SDR; * p < .05 vs Vehicle/Wistar; ^ p < .05 vs MCT/SDR two-way ANOVA with Tukey's multiple comparison test.

Figure 2. MCT-induced RV Structural Changes Were More Pronounced in SDR



RV dilation was observed with MCT treatment, as quantified by higher RV end-diastolic area (RVEDA) and RV end-systolic area (RVESA) in MCT/SDR and MCT/Wistar as compared with the respective vehicle controls. RV dilation was greater in MCT/SDR as compared to MCT/Wistar rats. RV dilation was confirmed by an increased RV internal diameter during diastole (RVIDd) and systole (RVIDs) in MCT/SDR as compared to vehicle/SDR and MCT/Wistar rats.

MCT/SDR also exhibited RA dilation (right atria area [RAA] increase) as compared to vehicle/SDR and MCT/Wistar rats. An increase in the RV free wall thickness (RVFWT) was also observed in the MCT-treated rats.

Values are expressed as mean ± SD. # p < .05 vs Vehicle/SDR; * p < .05 vs Vehicle/Wistar; ^ p < .05 vs MCT/SDR two-way ANOVA with Tukey's multiple comparison test.

Figure 3. MCT-induced Decrease in PAT/CL Ratio Was Greater in SDR



MCT treatment induced decreases in the pulmonary acceleration time (PAT) normalized by cycle length (CL) ratio and in the pulmonary acceleration time (PAT) normalized by pulmonary ejection time (PET) ratio in MCT/SDR and MCT/Wistar as compared with the respective vehicle controls. A greater decrease in PAT/CL was observed in SDR as compared to Wistar rats.

Values are expressed as mean ± SD. # p < .05 vs Vehicle/SDR; * p < .05 vs Vehicle/Wistar; ^ p < .05 vs MCT/SDR two-way ANOVA with Tukey's multiple comparison test.

Figure 4. MCT-induced RV Systolic Dysfunction Was Prominent in SDR



RV function was decreased with MCT treatment in both strains, but RV dysfunction was more prominent in MCT/SDR than MCT/Wistar rats as shown by a greater decrease in RV fractional area change (RVFAC) in MCT/SDR.

MCT treatment also showed a decrease in tricuspid annular plane systolic excursion (TAPSE) and tissue Doppler-derived peak systolic velocity (s') in both strains as compared with the respective vehicle controls.

Values are expressed as mean ± SD. # p < .05 vs Vehicle/SDR; * p < .05 vs Vehicle/Wistar; ^ p < .05 vs MCT/SDR two-way ANOVA with Tukey's multiple comparison test.

Table 2. MCT-induced Decrease in CO and SV Was Greater in SDR

| PV-Loop Parameters | Experimental Groups | | | | | | | |
|------------------------|---------------------|---|------------------------------|---|-----------------------------|---|------------------------------|----|
| | Vehicle/SDR | | MCT/SDR | | Vehicle/Wistar | | MCT/Wistar | |
| | mean ± SD | n | mean ± SD | n | mean ± SD | n | mean ± SD | n |
| Body Weight Range (kg) | 0.345–0.431 | 8 | 0.223–0.290 | 7 | 0.273–0.347 | 9 | 0.230–0.293 | 11 |
| RV Pes (mmHg) | 23.02 ± 3.69 | 8 | 60.13 ± 4.26 [†] | 5 | 27.47 ± 4.09 | 9 | 55.09 ± 17.18 [*] | 10 |
| RV Pdev (mmHg) | 25.81 ± 1.02 | 8 | 61.80 ± 2.61 [†] | 5 | 30.00 ± 2.76 | 9 | 55.20 ± 17.05 [*] | 10 |
| HR (bpm) | 329.07 ± 33.15 | 8 | 297.08 ± 40.72 | 5 | 416.46 ± 33.96 [†] | 9 | 373.37 ± 46.25 [*] | 10 |
| RV CO (µL/min) | 178431 ± 40477 | 8 | 83259 ± 45809 [†] | 5 | 161964 ± 25469 | 7 | 118831 ± 34276 ^{**} | 10 |
| RV SV (µL) | 522.06 ± 162.25 | 8 | 277.00 ± 128.07 [†] | 5 | 392.16 ± 59.51 [†] | 7 | 313.29 ± 67.05 ^{**} | 10 |
| Ees/Ea ratio | 0.52 ± 0.24 | 8 | 0.84 ± 0.34 | 5 | 0.42 ± 0.13 | 6 | 0.69 ± 0.27 | 10 |
| Ees (mmHg/µL) | 0.022 ± 0.011 | 8 | 0.217 ± 0.143 [†] | 5 | 0.029 ± 0.007 | 6 | 0.131 ± 0.076 | 10 |
| Eed (mmHg/µL) | 0.009 ± 0.010 | 5 | 0.005 ± 0.004 | 5 | 0.001 ± 0.001 | 4 | 0.008 ± 0.010 | 9 |
| Ea (mmHg/µL) | 0.04 ± 0.01 | 8 | 0.25 ± 0.10 [†] | 5 | 0.07 ± 0.01 | 7 | 0.19 ± 0.10 [*] | 10 |

SDR, Sprague Dawley rats; HR, heart rate; RV Pes, right ventricle end-systolic pressure; RV Pdev, right ventricle developed pressure; RV CO, cardiac output; RV SV, right ventricle stroke volume; Ees/Ea, RV-vascular coupling; Ees, end-systolic elastance; Eed, end-diastolic elastance; Ea, arterial elastance; Monocrotaline (60 mg/kg) as a single dose administered on Day 0.

RV catheterization showed similar MCT-induced increases in RV end-systolic (RV Pes) and developed pressure (RV Pdev) in both strains. However, the decrease in cardiac output (CO) and stroke volume (RV SV) was greater in MCT/SDR than in MCT/Wistar rats.

No change in RV contractility as measured by end-systolic elastance (Ees), RV stiffness as measured by end-diastolic elastance (Eed) and the RV-vascular coupling (Ees/Ea Ratio) was observed with MCT treatment in either strain. However, arterial elastance (Ea) was increased with MCT treatment in both strains as compared to the respective vehicle controls.

Values are expressed as mean ± SD. # p < .05 vs Vehicle/SDR; * p < .05 vs Vehicle/Wistar; ^ p < .05 vs MCT/SDR two-way ANOVA with Tukey's multiple comparison test.

Conclusion

Our results showed that while similar hemodynamic changes were observed in SDR and Wistar rats in response to MCT, the magnitude of dilated RV hypertrophy and systolic impairment was exacerbated in SDR as compared to Wistar rats.